A new 1D velocity model and absolute locations image the Mayotte seismo-volcanic region

Aude Lavayssière, Wayne C. Crawford, Jean-Marie Saurel, Claudio Satriano, Nathalie Feuillet, Eric Jacques, J. C. Komorowski

Journal of Volcanology and Geothermal Research 421 (2022) 107440

Contents lists available at ScienceDirect

Journal of Volcanology and Geothermal Research

journal homepage: www.elsevier.com/locate/jvolgeores

A new 1D velocity model and absolute locations image the Mayotte seismo-volcanic region

Aude Lavayssière *, Wayne C. Crawford, Jean-Marie Saurel, Claudio Satriano, Nathalie Feuillet, Eric Jacques, Jean-Christophe Komorowski

Université de Paris, Institut de Physique du Globe de Paris, CNRS, F-75005 Paris, France

ARTICLE INFO

Article history:
Received 31 May 2021
Received in revised form 10 November 2021
Accepted 17 November 2021
Available online 20 November 2021

Keywords:
Volcano seismicity
Mayotte
Magmatic plumbing system
Eruption dynamic

ABSTRACT

In May 2018, a seismically quiet region of the Indian Ocean awoke. More than 130 magnitude 4+ earthquakes were recorded in the first month, including a M_W 5.9 event on May 15th, 2018. This seismic activity was later identified as being related to an exceptional underwater volcanic eruption offshore Mayotte island, which had emitted more than 6.5 km^3 of lava by the time of writing. To better constrain the geodynamic processes responsible for the seismic and volcanic activity, a new network of ocean-bottom seismometers and land stations has been deployed around the seismically active region since February 2019. We present here an improved 1D velocity model for the active area and relocations of manually-picked earthquakes using this new model. The best-constrained events image detailed structures within two clusters of seismic activity east of Mayotte. The westernmost, proximal cluster, close to Mayotte's Petite-Terre island, has a "donut" shape horizontally and an "hourglass" shape in depth. The events distribution suggests the presence of a magma reservoir at around 27 km depth, with earthquakes focused along its sides, and a collapsing system underneath, related to the drainage of another, deeper magma storage zone. The distal cluster, focused 30–50 km offshore of Petite-Terre island, highlights the propagation of a dike between 45 and 25 km depth, aligned towards the new volcanic activity on the seafloor. We interpret this cluster as the fluid pathway towards the new volcano and nearby active seafloor lava fields. The improved velocity model also permits more robust daily monitoring of the seismicity using land stations, allowing local authorities to better assess seismic and volcanic hazards and to communicate them to the island's population.

1. Introduction

In seismically active regions, a precise analysis of the spatial distribution of seismicity is invaluable for characterizing active structures and current stresses. The precision and accuracy of absolute earthquake locations depend on the network geometry, data quality and on having an accurate velocity model of the subsurface (i.e., information on the lithospheric structure below the stations; Crosson, 1976; Gomberg et al., 1990; Kissling, 1988; Kissling et al., 1995; Pavlis, 1986; Thurber, 1983).

Determining the structure of a volcanic system can be even more challenging than in other regions, as volcanoes are complex structures with many heterogeneities due to their magmatic system and the accumulation of different materials from successive eruptions. This structure contributes to the dynamics of any future eruption, such as magma intrusion or ground deformation. An accurate velocity model - and hence precise hypocenter locations - around volcanic systems is crucial for the monitoring and interpretation of observations associated with magma migration or active structures (e.g., Mount Etna volcano: Chiarabba et al., 2000; Aloisi et al., 2002; Taupo Volcanic Zone: Clarke et al., 2009; Piton de La Fournaise: Lengliné et al., 2016; Kanlaon volcano: Sevilla et al., 2020; Taal volcano: You et al., 2013, 2017).

Because the region around Mayotte was, historically, seismically quiet (Bertil and Regnoult, 1998), local subsurface velocity information was sparse before the 2018 Mayotte activity. Previous models include: 1) a regional P-wave velocity profile, hereafter named the "Coffin" model, from a 1980 active-seismic sonobuoy experiment 100 km southeast of Mayotte (instrument 449, Coffin et al., 1986) (Fig. 1), completed for depths >10 km by a bibliographic study concerning the crustal structure of the Somali basin and the Mozambique channel (Jacques et al., 2019; Saurel et al., 2021a; Leinweber et al., 2013; Phethean et al., 2016); and 2) an S-wave velocity profile (Dofal et al., 2018, 2019, 2021), hereafter named the "ADofal" model, obtained using receiver functions at a temporary station (MAYO) on Mayotte, deployed as part of the 2012–2013 RHUM-RUM experiment (Barruol et al., 2012)

* Corresponding author.
E-mail address: lavayssiere@ipgp.fr (A. Lavayssière).

https://doi.org/10.1016/j.jvolgeores.2021.107440

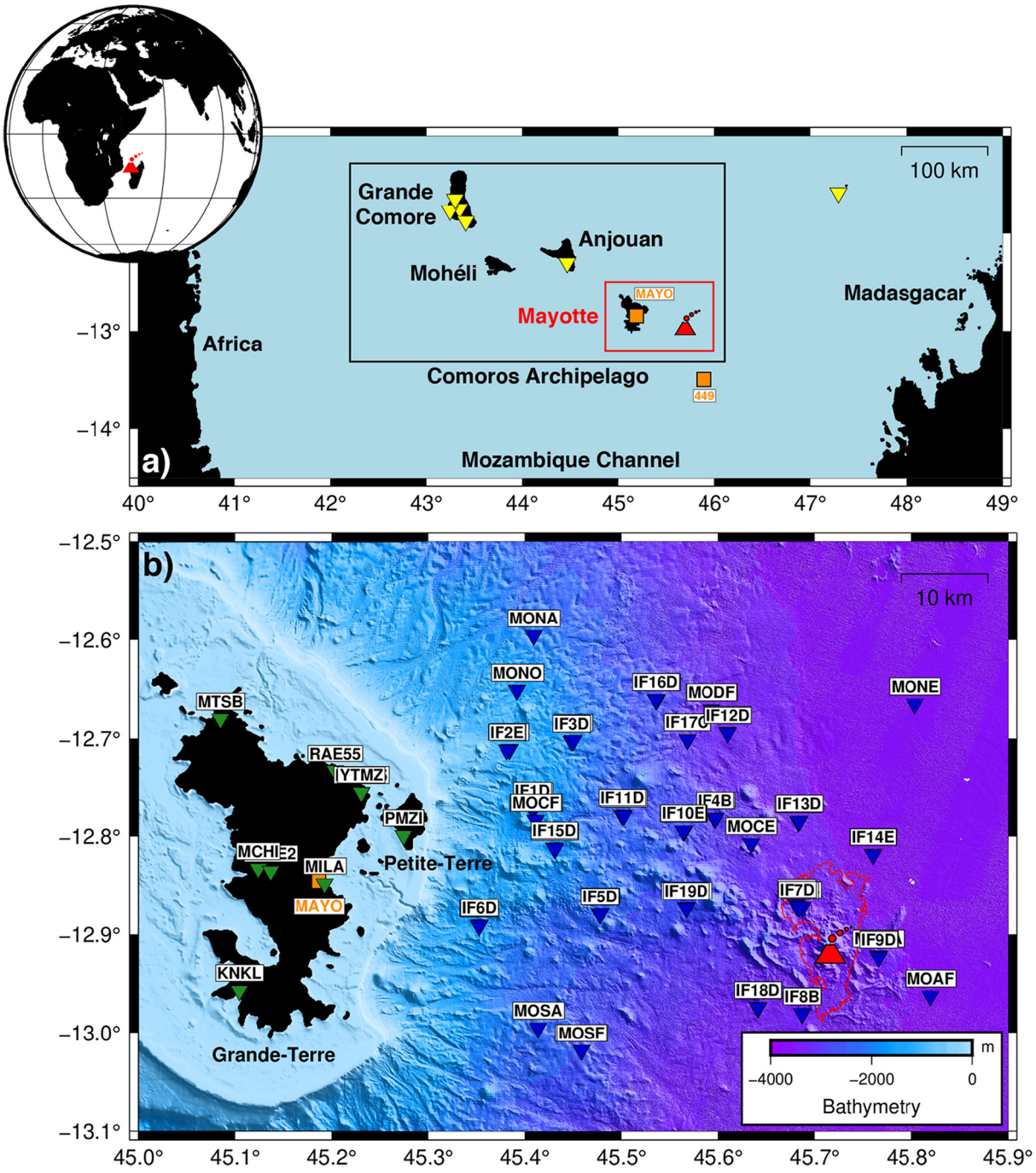

Fig. 1. a) Location of the study area (red rectangle) in the Mozambique Channel. The inset shows the area in a global context as a red volcano symbol. Yellow inverted triangles are regional stations used in the relocation. Orange squares are instruments used for other studies (see main text for details). b) Map of the seismic network deployed between Mayotte and the NVE (red volcano symbol). The extent of the integrated cumulative lava flows field related to the actual eruption, as of 17-01-2021, is indicated as a red contour (Feuillet et al., 2021; Rinnert et al., 2019; REVOSIMA, 2021). The green inverted triangles represent the land stations; the blue inverted triangles represent the OBSs.

(Fig. 1). The Coffin model places the Moho discontinuity at 13–15 km depth and infers a constant Vp/Vs ratio of 1.72, whereas the ADofal model places the Moho at ~17 km depth and yields a Vp/Vs ratio of 1.66.

In May 2019, the MAYOBS1 oceanographic campaign (Feuillet, 2019) investigated the Mayotte seismic activity and discovered a new volcanic edifice (NVE) 50 km ESE of Mayotte's Petite-Terre island (Feuillet et al., 2019, 2021) (Fig. 1). During this expedition, the scientists recovered 6 Ocean-Bottom Seismometers (OBS), deployed in late February 2019, and the seismology team onboard developed a 1D hybrid velocity model to better constrain the location of the earthquakes (Saurel et al., 2021a). This first local velocity model, hereafter named the "MAYOBS1" model, uses the ADofal model for local stations (OBSs and Mayotte land-based stations, Dofal et al., 2018, 2019, 2021), the Coffin model for regional stations (Comoros and Glorieuse islands, 200–400 km from Mayotte) and the global ak135 model (variable V_P/V_S, Kennett et al., 1995) for more distant stations (Madagascar, Africa or the Indian Ocean) (Saurel et al., 2021a). This hybrid model was built using sparse data, including the first OBS deployment which had a very large aperture because of the pre-existing uncertainty on

the earthquake locations. The locations obtained using this model greatly improved the earthquake location accuracy (e.g., Feuillet et al., 2021), but some stations still had relatively high residuals (> 0.8 s for S-wave arrival times at the westernmost land-stations and for earthquakes further than ~30 km from Mayotte island).

To continuously monitor the seismic activity in the region, a team of scientists from the REVOSIMA observatory (REseau de surveillance VOlcanologique et SIsmologique de Mayotte; REVOSIMA, 2021) picks and locates the earthquakes daily using land-station data. Once the OBSs are recovered, these events are then manually re-picked to improve their locations. This processing revealed the inadequacy of the velocity model, as locations made using only land data were moved by up to 10 km to the northeast when the OBS picks were added. As the local communities, scientists and decision-makers need accurate, near-real time locations, it became clear that the model needed to be improved.

We describe here the development of a more accurate 1D velocity model that improves locations, particularly for earthquakes located far from Mayotte. This model greatly improves real-time monitoring, by significantly reducing location errors using only the land-based network. It also provides much sharper images of the seismicity distribution when the OBS data is added. We present the absolute locations obtained with this new model and show that they image the detailed structures responsible for Mayotte's on-going (at the time of writing) seismo-volcanic activity. Based on our observations and recently published studies, we propose an updated interpretation of the volcanic plumbing system feeding the new eruption.

2. Geological and tectonic settings

The Comoros archipelago, in the Mozambique Channel, is composed of four islands: Grande Comore, Mohéli, Anjouan and Mayotte, all roughly EW aligned. The cause of the volcanic and magmatic activity in this region is debated, with hypotheses ranging from the interaction of a mantle plume with the oceanic lithosphere (Claude-Ivanaj et al., 1998; Emerick and Duncan, 1982; Hajash and Armstrong, 1972) to lithospheric movements related to East African Rift dynamics (Lemoine et al., 2020; Michon, 2016; Nougier et al., 1986). It is suggested that the EW alignment of the islands is due to a plate boundary between the Lwandle and Somalia plates (Famin et al., 2020; Saria et al., 2014; Stamps et al., 2018; Feuillet et al., 2019, 2021), or it indicates a transtensional transfer zone between the offshore branch of the East African Rift and the graben in Madagascar (Feuillet et al., 2019, 2021).

The nature of the crust north of the archipelago is suggested to be oceanic and dating back to the Mesozoic (Davis et al., 2016; Malod et al., 1991; Rabinowitz et al., 1983; Sauter et al., 2018; Segoufin and Patriat, 1981), while in the south it is highly debated, between a thinned continental crust (e.g., Bassias and Leclaire, 1990; Flower and Strong, 1969) and a Jurassic oceanic crust (e.g., Phethean et al., 2016; Klimke et al., 2016; Rabinowitz et al., 1983; Talwani, 1962).

Mayotte is the easternmost and oldest island of the archipelago, with the onset of its volcanic onshore activity dated at 11 Myrs (Debeuf, 2004; Emerick and Duncan, 1982; Hajash and Armstrong, 1972; Nougier et al., 1986; Pelleter et al., 2014) and the onset of its submarine activity estimated at 20 Myrs (Michon, 2016). The current Mayotte seismic activity started in May 2018, when over 130 $M_L > 4$ earthquakes occured in one month, including a M_W 5.9 event on May 15th, 2018 (Cesca et al., 2020; Lemoine et al., 2020). This activity is on-going as of this writing, and almost 1000 $M_L > 4$ events have been recorded between the beginning of the activity and January 1st, 2021. Such an intense, strong and long-lived seismicity has never before been recorded in the Comoros archipelago. Associated with the seismicity, subsidence and eastward displacement have been observed on land since July 2018 and several very long period (VLP) seismic events were also detected (e.g., Feuillet et al., 2021; Cesca et al., 2020; Lemoine et al., 2020). The VLP events have been interpreted as evidence of fluid migration/resonance related to the possible withdrawal of magma from a reservoir (Cesca et al., 2020; Lemoine et al., 2020, Feuillet al., 2021), a hypothesis that was then supported by the discovery of the 820 m-high submarine NVE in May 2019 (Feuillet et al., 2021).

At least 6.55 km^3 of lava has erupted as of May 2020, forming the NVE and other lava flows (red contour, Fig. 1), and making this the largest submarine eruption ever documented (Feuillet et al., 2021). Petrology and geobarometry data suggest that this lava originates from a deep (36.8–48 ± 10 km), large (> 9.3 km^3) mantle reservoir of alkaline, volatile-rich, magma that evolved and experienced high crystallization (Berthod et al., 2021a). The magma ascent towards the NVE sampled a shallower reservoir (17.1 ± 6.5 km depth), probably from previous activity (Berthod et al., 2021a). More recently, in May 2020, new lava flows were observed a few kilometers to the NW of the NVE, spreading over 5 km^2 (REVOSIMA, 2021; Rinnert et al., 2019) (Fig. 1).

As studies progress since the start of the activity, most-likely scenarios have been developed (Cesca et al., 2020; Lemoine et al., 2020). They propose that the first phase of seismicity, between May 10th and May 31st, 2018, was caused by the fracturing of the crust without magma intrusion; then, in June 2018, the injection of magma in fissures started with a week of intense seismic activity and its migration to the SE (Cesca et al., 2020; Lemoine et al., 2020; Feuillet et al., 2021). The eruption is thought to have started in early July with the apparition of the NVE on the seafloor (Feuillet et al., 2021). As of September 2018, there are two clusters of seismicity - one to the east, closer to the new volcano, and one to the west, closer to Mayotte - and both are still active at the time of writing. Ground deformation modeling showed that the magma likely comes from a deflating reservoir at ~30 km (Cesca et al., 2020; Lemoine et al., 2020) or ~ 50–55 km depth (Feuillet et al., 2021). This deflating reservoir is thought to reactivate subvertical faults responsible for the cluster close to Mayotte (Cesca et al., 2020; Feuillet et al., 2021).

After more than 2 years, the seismicity, ground deformation and emission of lava persist, with a large number of smaller earthquakes, often associated with long-period and very long-period events (Cesca et al., 2020; Poli, 2019; Satriano et al., 2019; Feuillet et al., 2021; Rinnert et al., 2019; REVOSIMA, 2021).

3. Seismic network and catalog

Since the end of February 2019, networks of OBSs have been deployed during the MAYOBS oceanographic campaigns (Saurel et al., 2021a; Rinnert et al., 2019). Every 3 to 4 months, the OBSs are recovered then re-deployed on some of the 27 sites occupied between Petite-Terre island and the site of the new eruption (Fig. 1, Saurel et al., 2021a). In total the OBSs plus land-based stations network covers an area of ~100 km × 60 km (Fig. 1) that includes most of the known geological and tectonic structures representative of Mayotte's historic volcanic activity.

This network recorded close to 100,000 earthquakes between February 2019 and May 2020 and 4254 of these events were manually picked on both the land stations and the OBSs (Saurel et al., 2021a, 2021b). These 4254 events, with M_L ranging from 0 to 5.53 (M_C ~ 3), form the base catalog for our analysis.

4. Development of a 1-D velocity model

4.1. Data selection

In order to accurately locate earthquakes, a good velocity model representing the subsurface structure of the study area is essential. We used the program VELEST (Kissling et al., 1995) to develop a best-fit "minimum" 1D velocity model and estimate station corrections by minimizing the misfit between the arrival times and model predictions.

We selected the dataset used to develop this "minimum" 1D velocity model by taking the highest-quality events from the catalog of manually-located events. We performed a preliminary location analysis

using NonLinLoc (Lomax et al., 2000; Lomax et al., 2014) and the MAYOBS1 model (Saurel et al., 2021a). We then selected events with: at least 30 phases recorded on local and regional stations; an azimuthal gap of less than 180°; a horizontal location error of less than 2 km and a vertical location error of less than 5 km. This selection yields 813 events (Fig. 2), whose local magnitudes range from 1.1 to 5.5. A weighting factor w was assigned to each phase to represent the uncertainties u of the manually picked arrivals: $w = 0$ represents u ≤ 0.01 s; $w = 1$ represents u = 0.01–0.05 s; $w = 2$ represents u = 0.05–0.1 s; $w = 3$ represents u = 0.1–0.2 s; and w = 4 represents u ≥ 0.2 s.

In order to remove any inconsistent picks and to quantify the Vp/Vs ratio of the dataset, we plotted the arrival times on Wadati diagrams (Fig. S1 Supp Mat). Any arrival pick significantly offset from the slope line was removed from the catalog. The Wadati diagram indicates a Vp/Vs of 1.73 at regional distances (Fig. S1a Supp Mat) and 1.65 at local distances (< 15 s P-wave travel time) (Fig. S1b Supp Mat). These results correlate well with previous studies for regional and local distances (Coffin et al., 1986; Dofal et al., 2018, 2019; Dofal et al., 2021; Saurel et al., 2021a). The low Vp/Vs value for the study area could be evidence for thick sedimentary layers, undamaged oceanic crust, presence of gas, or the presence of old cooled magmatic conduits.

4.2. « Minimum » 1-D velocity model

VELEST inverts the travel times in a trial-and-error process to minimize the residual RMS, and uses a set of parameters chosen by the user. For our study, we use both P- and S-wave travel time data and the initial models used as initial inputs are 1) a new "ADofal" model from an updated receiver function analysis of the region (green, Fig. 3) (Dofal et al., 2021) and 2) the MAYOBS1 model (black, Fig. 3) (Saurel et al., 2021a). The other parameters chosen by the user are the reference station (YTMZ for its central location), the number of iterations in each run (20) and the fact that we use the station corrections calculated by VELEST in each subsequent iteration. To avoid computational instabilities, we also also impose that velocity grows monotonically with depth (i.e., no low-velocity zones are allowed in the model).

In the first run, VELEST calculates a velocity model, performs the relocations and calculates station corrections for each of the initial velocity models. Hence, the final number of layers is the one from the initial models. From the results of these inversions (one for each initial model), we look at the best model - i.e., the resulting model with the smallest RMS - and verify that it has coherent values, depending on general knowledge and on local information. From the chosen model, we combine the layers with same or very close velocities - hence slightly changing the layering -, and input this model as the new initial model in the next run. Note that we do not combine layers of similar velocities if they form a gradient, such as the one between 15 and 20 km in our case. From the second run we also use the estimated station corrections as input in the next run. We keep doing this process until the RMS and velocity model don't change anymore in the next runs. Further tests of the stability of this last model are presented in Fig. S2 Supp Mat (Kissling et al., 1995; e.g., Matrullo et al., 2013; Lavayssière, 2019). At the end of all the runs and tests, the RMS decreased from 0.645 s for the ADofal model to 0.163 s in our final "minimum" 1D velocity model, hereafter named "ALav" (red model, Fig. 3).

The new velocity model has slower velocities than the previous models in the first 10 km and higher velocities below the Moho (depths >17 km), closer to "normal" mantle velocities (~8 km/s, e.g. Pasyanos et al., 2014). The Vp/Vs ratio is relatively high (~1.8) between 3 and 10 km depth and low (~1.6) beneath. These results will be discussed further in the Discussion section.

VELEST also calculates travel time corrections at each station. These station corrections account for lateral variations in the velocity structure, particularly at shallow depths beneath the stations, such as variations in the sedimentary sequences. The calculated station corrections are relatively high, hinting that there are strong near-surface lateral heterogeneities, and we therefore include them in our location algorithm.

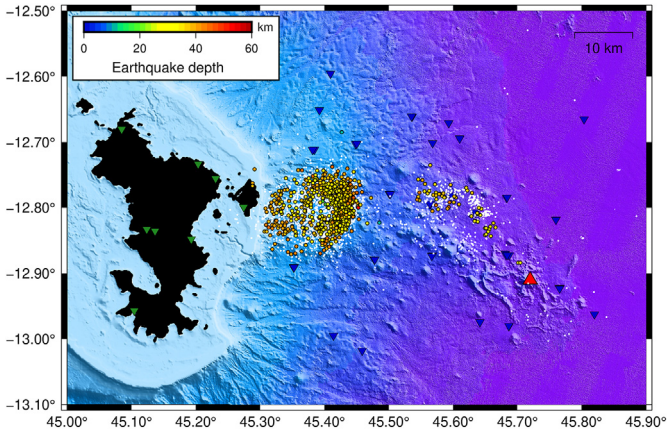

Fig. 2. Events selection. White dots = full catalog (Saurel et al., 2021b), colored dots = selected events colour-coded by depth. The green inverted triangles represent the land stations; the blue inverted triangles represent the OBSs; the red triangle marks the location of the NVE.

5. Catalog relocations

5.1. Location improvements

We used the new ALav velocity model and VELEST station corrections to relocate the 4254 manually-picked events from February 2019 to May 2020. We ran NonLinLoc (Lomax et al., 2000; Lomax et al., 2014) several times, reinjecting new station corrections calculated by NonLinLoc at every run, until the RMS and the station residuals stopped varying significantly (< 0.01 s mean variation).

To evaluate the improvement in event locations obtained with the new velocity model and the final station corrections (Fig. S3 Supp Mat), we compare NonLinLoc results using the ALav model to a NonLinLoc run using the MAYOBS1 velocity model (Fig. 4). The results show that the errors in location are reduced using the new model, with the RMS significantly reduced, the horizontal errors also reduced, and no change in the depth errors which suggests that the depth constraint is independent of which velocity model is used.

We further evaluate the uncertainty in depth and location by examining relocations done using only nearby or only distant stations, and relocations done using only P-arrivals (Fig. S4 Supp Mat). These tests show that the depth is well-constrained as the majority of the events' depths are not varying significantly whichever relocation parameters we use. Only relocations with distant stations show large variations in depth and locations, as well as a fewer number of earthquakes relocated, as expected. The depth constraint is particularly good for the proximal cluster (Fig. S4a Supp Mat) but slightly less so for the distal cluster as the relocations using the new model with only P-arrivals or using the MAYOBS1 velocity model both result in the distal events being ~5 km deeper than our results (Fig. S4a Supp Mat). There is however a clear improvement in the overall locations as we see more tightly clustered events with the full relocation compared to all other relocation methods (Fig. S4b Supp Mat).

Event locations are also better constrained with the new 1D velocity model and station corrections when using only data from the land stations, representative of the continuous monitoring (Fig. 5). The improvement using the new velocity model is particularly clear for the distal cluster, which the previous model located near to the proximal cluster (dark gray circles, Fig. 5a). With the new model, land-based locations (white circles, Fig. 5b) are clustered over or close to their corresponding land-sea locations (red shapes, Fig. 5).

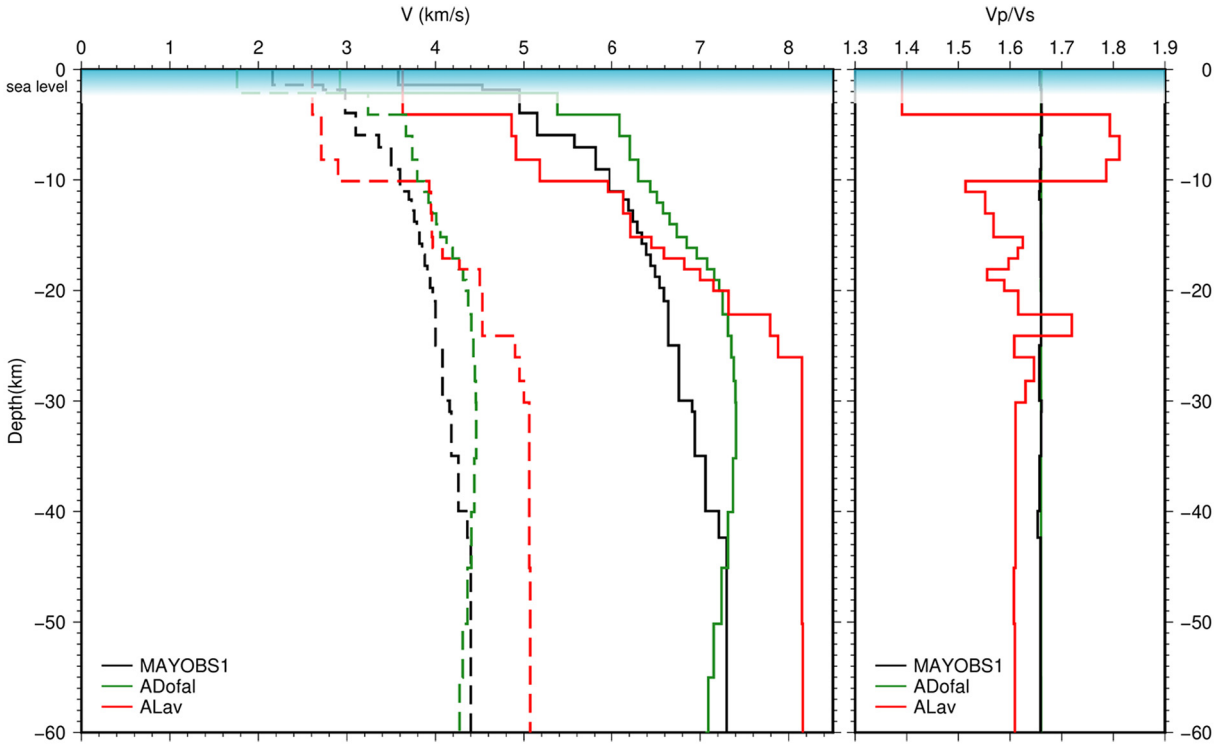

Fig. 3. Final ALav 1D velocity model and Vp/Vs ratio (red lines) compared to the initial ADofal (green lines, Dofal et al., 2021) and MAYOBS1 (black lines, Saurel et al., 2021a) velocity models and Vp/Vs ratios. Note that 0 depth is the sea level.

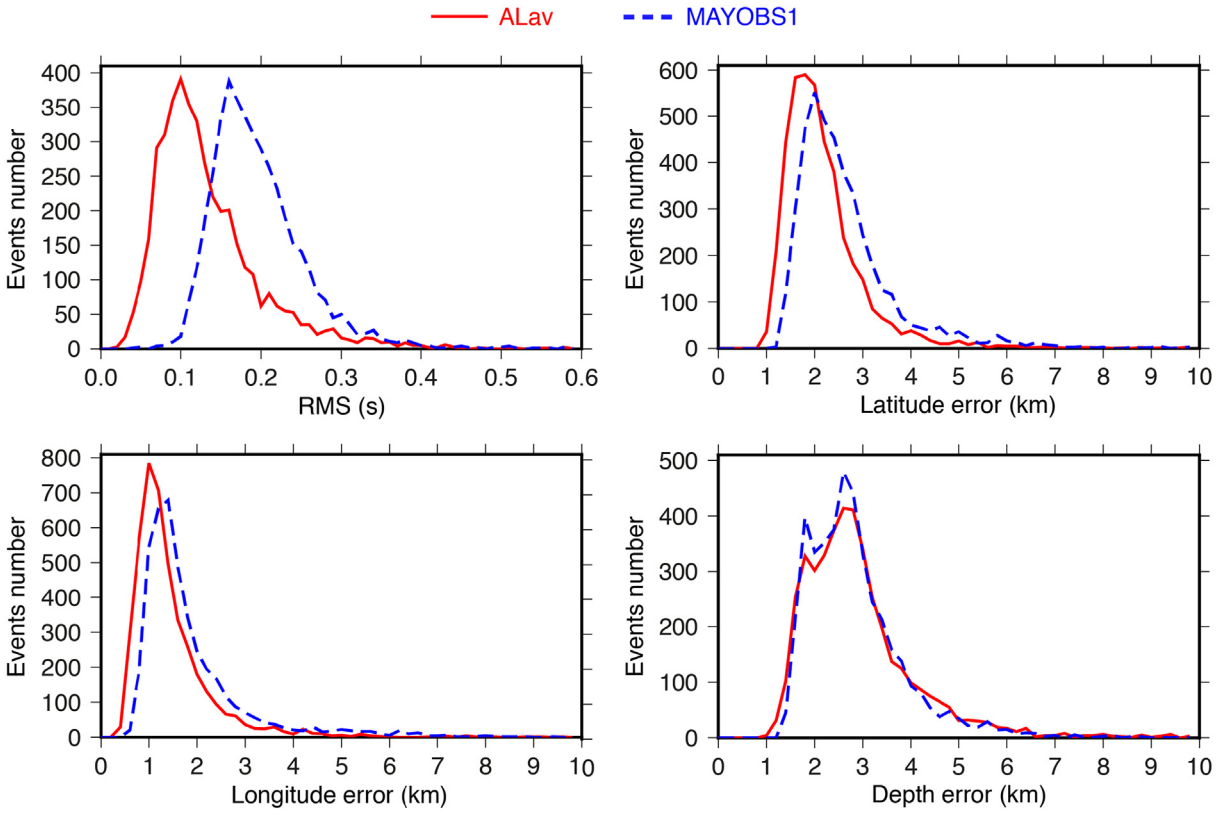

Fig. 4. RMS and locations errors distributions for the ALav model (red) and for the MAYOBS1 model (blue; Saurel et al., 2021a).

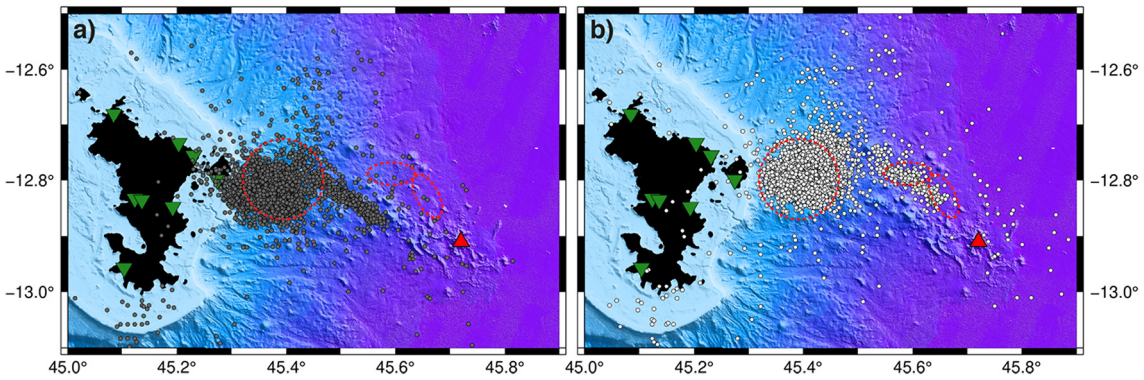

Fig. 5. Events' locations using only the land-stations network, representative of the daily monitoring. a) Events' locations with MAYOBS1 velocity model (dark gray circles, Saurel et al., 2021a); and b) Events' locations with the new ALav model (white circles). The red dashed shapes represent the locations of the seismic clusters when located with the new model and both the land-based and OBSs data. The green inverted triangles represent the land stations; the red triangle marks the location of the NVE.

5.2. Absolute locations

From the base catalog of 4254 events, we select a subset of 3445 "best" events, with horizontal errors <2.5 km and vertical errors <5 km, in order to study and interpret the best-constrained seismic structures beneath offshore Mayotte (Fig. 6). To illustrate the improvement in delineated structures obtained with the new model, we also present in Fig. S6 Supp Mat a map and several cross-sections of the best-constrained seismicity located with the MAYOBS1 model using the same selection by locations errors. Note that because the MAYOBS1 model is not as good as our model, there are fewer events that match the same location quality criteria (Fig. S6 Supp Mat).

The two previously-identified proximal and distal clusters of seismicity (Cesca et al., 2020; Lemoine et al., 2020; Feuillet et al., 2021; Saurel et al., 2021a) are more tightly clustered and better reveal deep structures. Both clusters do not seem connected in our dataset.

The proximal cluster contains the majority of the seismicity and is close to Mayotte, a few kilometers from Petite-Terre island, home to Mayotte's airport and its major administrative and energy centers (Fig. 6). The events are distributed in a "donut" shape with a ~ 4 km-diameter aseismic center at 45.4°W and 12.8°S (Fig. 6). This circular distribution is particularly clear on the cluster's eastern side, which also hosts the largest events (Fig. 6). On the western side, closer to Petite-Terre, the events are smaller and more spatially scattered (Fig. 6).

Fig. 7 shows four cross-sections through the proximal cluster. A first observation is that the proximal cluster forms an "hourglass" shape, centered at ~35 km depth (clearest on Profile AA', Fig. 7a). The events in the top part of this hourglass seem distributed around a roughly oval shape, centered at ~27 km depth (light red shape, clearest on Profiles AA' and CC', Fig. 7a and b). The bottom part of the hourglass is composed of more linear structures, with a few events scattered in the middle (Fig. 7). The eastern linear structure is more densely clustered

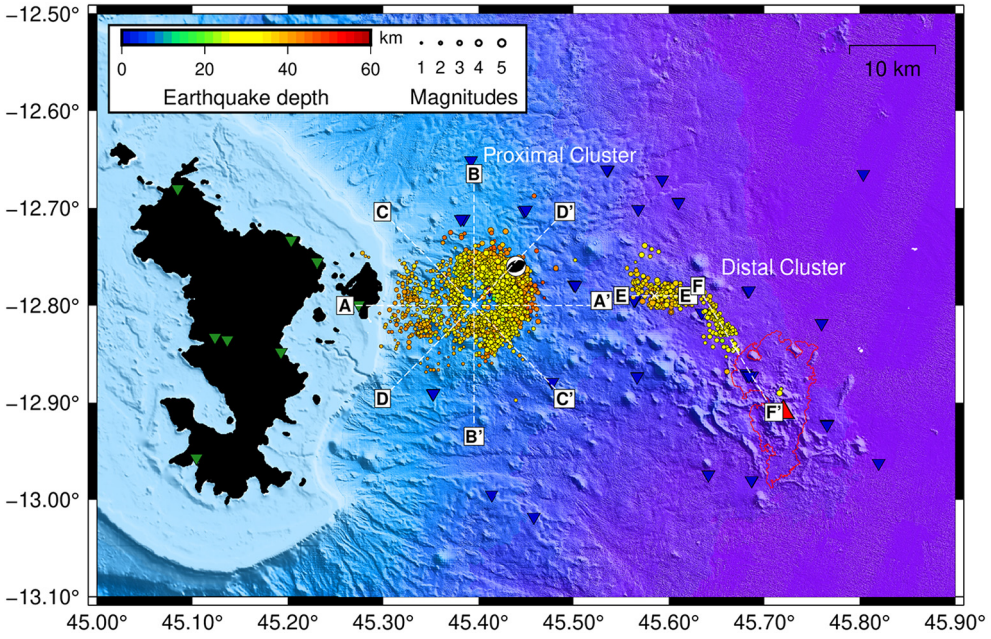

Fig. 6. Distribution of the best-constrained seismicity in the study area, colour-coded by depth and scaled by magnitudes, with traces of the cross-sections (dashed white lines) shown in Figs. 7 and 8. The focal mechanism of the May 14th, 2019 M_W 4.9 event, relocated with the new velocity model, is indicated. The green inverted triangles represent the land stations; the blue inverted triangles represent the OBSs; the red triangle marks the location of the NVE. The extent of the integrated cumulative lava flows field related to the actual eruption, as of 17-01-2021, is indicated as a red contour (Feuillet et al., 2021; Rinnert et al., 2019, REVOSIMA, 2021).

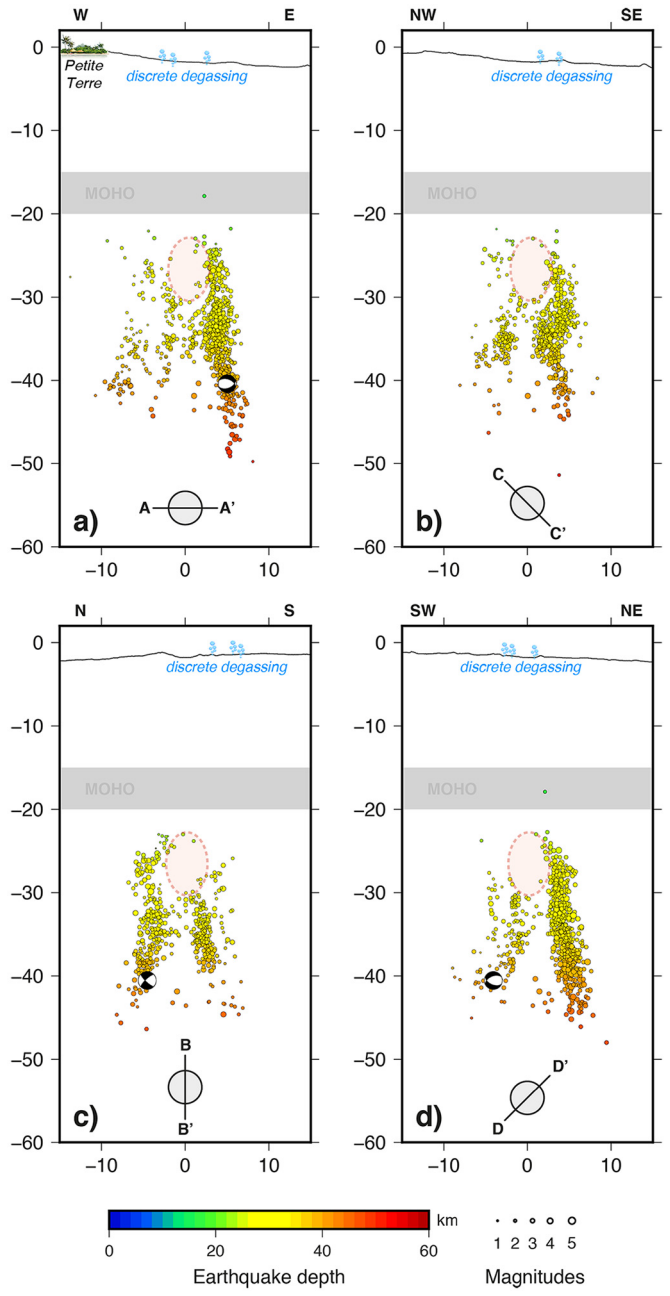

Fig. 7. 1.5 km-wide cross-sections across the proximal cluster with a) profile AA', b) profile CC', c) profile BB' and d) profile DD'. The earthquakes are colour-coded by depth and scaled by magnitude. The symbol at the bottom of each section represents the line of cross-section (line) though the cluster (circle). The Moho interface from the ALav velocity model is indicated in gray. The focal mechanism of the May 14th, 2019 M_W 4.9 event, relocated with the new velocity model, is indicated. The structure highlighted in light red is discussed in the text. Note that 0 depth is the sea level.

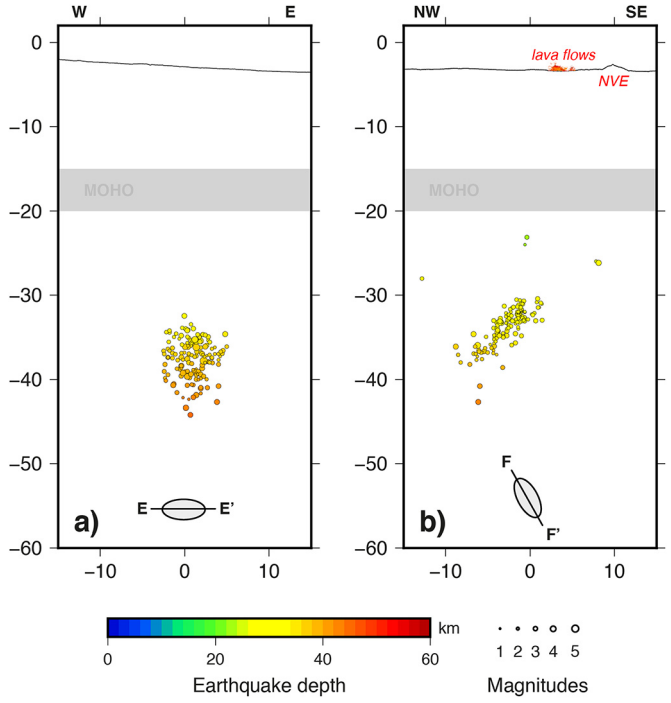

Fig. 8. 2 km-wide cross-sections across the distal cluster with a) profile EE' through the EW group and b) profile FF' through the N148 group. The earthquakes are colour-coded by depth and scaled by magnitude. The Moho interface from the ALav velocity model is indicated in gray. Note that 0 depth is the sea level.

and has more and bigger events than the western linear structure (Fig. 7a), including the May 14th, 2019 M_W 4.9 event whose moment tensor has been calculated (GCMT solution, Dziewonski et al., 1981; Ekström et al., 2012) and interpreted as a reverse motion (Feuillet et al., 2021) (Fig. 7). To the west, a second linear cluster, even closer to Petite-Terre, is visible between 42 and 30 km depth (Fig. 7a).

The distal cluster is composed of two smaller groups: an EW-aligned group (EE', Fig. 6) and a N148°E group (named N148) that is aligned towards the NVE (FF', Fig. 6). The aseismic region between the N148 group and the NVE correlates on the seafloor with new lava flows discovered a few kilometers to the NW of the NVE during the MAYOBS oceanographic cruises (Rinnert et al., 2019).

Fig. 8 shows cross-sections along both of these groups. The EW group spans depths from 45 to 32 km depth and has a slightly greater vertical than horizontal extent, but there is no clear structure (Fig. 8a). The N148 group events are clearly distributed along a NW-to-SE linear feature shallowing from 40 km at the NW to 30 km depth at the SE (Fig. 8b). There is almost no seismicity between 30 km depth and the seafloor in our dataset.

6. Discussion

We will not interpret in details the depth interfaces identified in the ALav model as we consider that the purpose of VELEST velocity models is mainly to improve earthquake locations. It does not take into account the 3D complexities of the region with probably large horizontal variations. However, the Vp/Vs obtained can provide insights on the nature of the crust and upper mantle beneath the study area. Unfortunately it does not resolve the debate over whether the crust is of continental or oceanic origin (e.g. Dofal et al., 2021; Bassias and Leclaire, 1990; Flower and Strong, 1969; Klimke et al., 2016; Rabinowitz et al., 1983; Talwani, 1962). Compared to the global crustal average Vp/Vs ratio of 1.75 (e.g. Christensen, 1996), the Vp/Vs ratio of ~1.8 between 3 and 10 km depth might either indicate a magmatic crust (Brocher, 2005), consistent with Mayotte's volcanic history, or an undamaged oceanic crust (Christensen, 1996; Guo et al., 2018). Below 10 km, the very low average Vp/Vs ratio of ~1.6 could be due to the presence of gas (Husen et al., 2004; Lin, 2013; Lin and Shearer, 2009; Guo et al., 2018), an increase in silica (Christensen, 1996; Zhang and Lin, 2014), an increase in water content (Lin and Shearer, 2009; Nakajima et al., 2001), or a more faulted crust (Mavko and Mukerji, 1998; Guo et al., 2018). Other volcanic regions show low Vp/Vs ratios due to an increase in isolated, low aspect-ratio, cracks caused by the presence of gas (e.g., El Hierro: López et al., 2017; Corbetti: Lavayssière, 2019; Kilauea: Johnson and

Poland, 2013; Mount Etna: Patanè et al., 2006; Campi Flegrei: Chiarabba and Moretti, 2006; Aso: Unglert et al., 2011). This is consistent with Mayotte's deformed crust due to volcanic activity and the associated migration of magma and fluids. It is also consistent with the gas-rich magma identified for the new eruption (Berthod et al., 2021a, 2021b). Note a slight increase in Vp/Vs ratio at ~23 km depth due to a decrease in S-wave velocity, too small to be fully interpreted but that could be caused by a narrow fluid-rich sill at the top of the proximal seismic cluster.

The new absolute locations of Mayotte seismicity reveal detailed structures in the crust and upper mantle offshore Mayotte. The top part of the proximal cluster partially outlines an ellipsoidal shape centered at ~27 km depth that could correspond to the magma reservoir inferred from the locations of VLP events (Feuillet et al., 2021; Lemoine et al., 2020) (Fig. 9). The sides of this inferred reservoir appear to be seismically active, which could be due to strains at the edges of the reservoir caused by its deformation (Fig. 9). The MAYOBS campaigns (Rinnert et al., 2019) have detected active degassing in discrete regions of the seafloor, slightly off-center from the center of the proximal cluster (REVOSIMA, 2021; Feuillet et al., 2021). This might mean that there is some gas migration from depth, possibly from the reservoir at 27 km depth indicated in this study (Fig. 9).

The linear structures at the bottom of the proximal cluster look very similar to ring faults caused by the deflation of a deeper reservoir (e.g., Geyer and Martí, 2014). Decreased pressure in a deflating reservoir could collapse its roof and create, or reactivate, overlying subvertical ring faults that would act in a reverse motion (Geyer and Martí, 2014). The focal mechanism of the May 14th, 2019 M_W 4.9 event (GCMT solution), mentioned by Feuillet et al. (2021) and relocated in the deep part of the proximal cluster with our velocity model, is consistent with the reverse outward-dipping motion on the ring faults defined by Geyer and Martí (2014) (Figs. 7, 9). From our relocations, the deeper deflating reservoir responsible for these faults would be located at depths greater than 45 km and would be consistent with the deflating reservoir inferred in previous works (Feuillet et al., 2021; Jacques et al., 2019; Berthod et al., 2021a, 2021b) (Fig. 9). This kind of subvertical ring faults have been observed during caldera collapse events (Acocella, 2007; Filson et al., 1973; Geshi and Oikawa, 2008; Gudmundsson et al., 2016) but these examples concern much shallower structures. In our case, the ring faults are exceptionally deep and there is an on-going debate about the possibility of a 40 km-deep collapsing system. Another hypothesis is that the load of the shallower reservoir at 27 km depth influenced the creation of these outward-dipping faults (e.g., Geyer and Martí, 2014). The alignment of the seismicity could also be caused by a layered system of magma lenses in an overall mush zone. In that case, the seismicity would be located at the edges of the lenses when they are (partially-)drained.

Possible other subvertical structures lie further to the west, almost beneath Petite-Terre island (Fig. 9). They appear to be too far from the rest of the seismicity to be part of the currently active ring faults but may be part of a larger, older structure. The deformation and change in the local stress created by the current eruption may have reactivated ancient structures further away (Fig. 9). These structures extend beneath Petite-Terre island, underlining the importance of monitoring the seismic activity in this region.

The distal cluster has been previously interpreted as a dike, feeding the surface activity (Cesca et al., 2020; Lemoine et al., 2020; Feuillet et al., 2021). Hence, it probably relates to the migration of magma

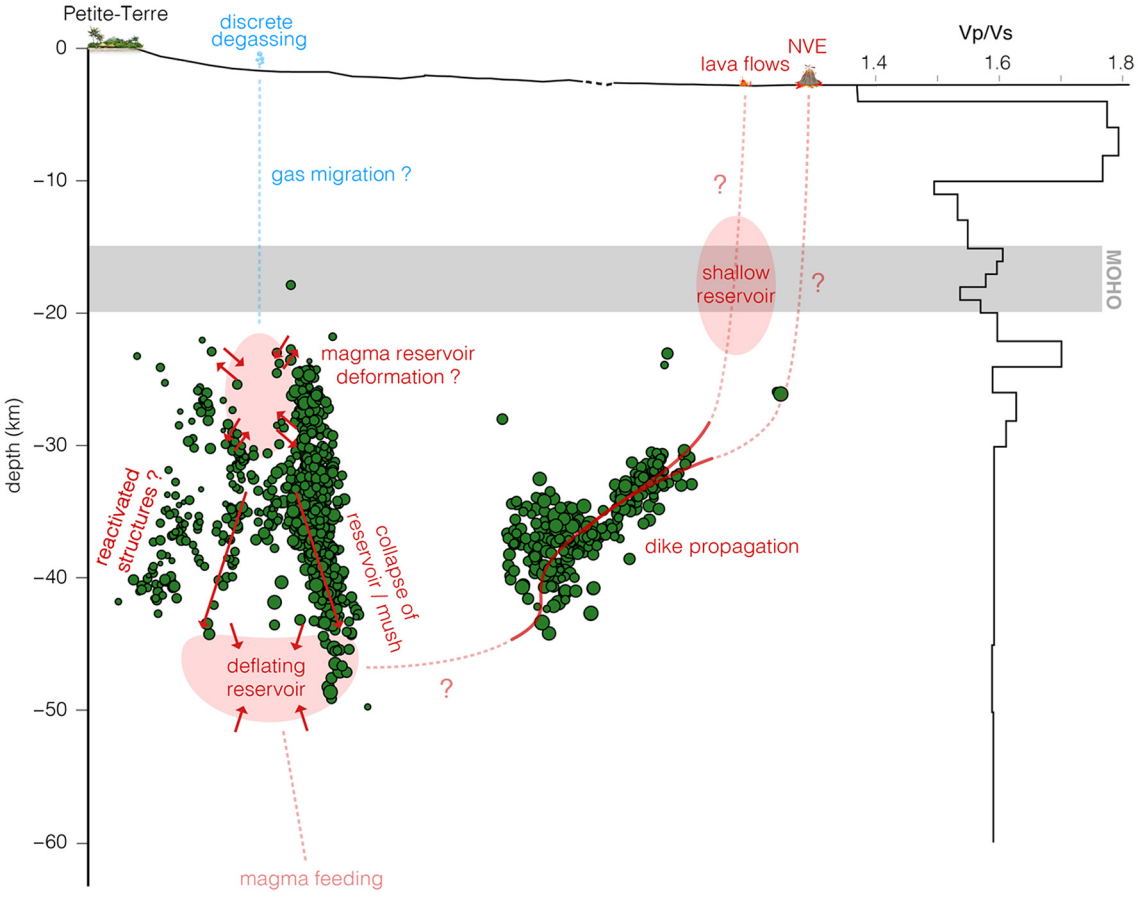

Fig. 9. Schematic interpretation using information from this study and the previous studies of Cesca et al. (2020); Lemoine et al. (2020); Feuillet et al. (2021), Saurel et al. (2021a); and Berthod et al. (2021a, 2021b). No vertical exaggeration.

and/or possibly of other fluids (Fig. 9). The EW-oriented group of this cluster is present throughout the OBS deployments, whereas the N148 group appeared after August/September 2019. This second sub-cluster could have been present beforehand and been masked (i.e., not detected) by the high energy activity of the proximal cluster, or it could be a new region of activity. The latter would then suggest that a conduit to the seafloor reopened - or a new path opened - around August/September 2019 towards the lava flow regions observed in May 2020. We believe that reopening of a pre-existing conduit is more likely, as there were previous clusters of activity in this region, although less accurately located (Lemoine et al., 2020).

Geobarometry results from analysis of rocks collected on the NVE indicates a probable reservoir at 17.1 ± 6.5 km depth beneath the NVE (Berthod et al., 2021a, 2021b), which could correlate with the abrupt ending of seismicity at 30 km depth, as the magma reaches a hotter and more ductile material (Priestley and McKenzie, 2006; Lavayssière, 2019; Woods et al., 2019) (Fig. 9). There is no seismicity between this reservoir and the surface, whether towards the NVE or towards the newest NW lava flows. Considering that the surface lava flows appear to be continuously active, the lack of seismicity could mean that the conduits reaching the surface are continuously open for magma migration, fed by this shallow reservoir. In contrast, as the distal cluster is continuously active, it is probable that the shallow reservoir beneath the NVE is fed discontinuously from the deeper reservoir beneath the proximal cluster, inferred in this study.

7. Conclusions

To better image and constrain the tectonic and volcanic structures responsible for Mayotte seismo-volcanic activity, we developed an improved local 1D velocity model using the recent network of land stations and OBSs deployed around the active region. This new velocity model allowed us to significantly improve the locations of 15 months of seismicity representative of the currently active volcanic system.

The relocations of all manually-picked earthquakes between February 2019 and May 2020 using the new velocity model and its associated station corrections confirm the presence of two main clusters of seismic activity and enhance details of their structure. The proximal cluster - from Petite-Terre island to ~20 km east offshore - is distributed in a “donut” shape horizontally and in an “hourglass” shape in depth. These forms suggest a possibly deforming magma reservoir centered at ~27 km depth and a collapsing system underneath due to the deflation of another magma storage zone at greater depths. The position of this cluster close to a populated island, although at several tens of km in depth, underscores the importance of monitoring this activity in real or near-real time, a monitoring which is greatly improved using the new velocity model.

The second, distal, cluster is located ~15 km further offshore from the proximal cluster. It is closer to but not beneath the NVE and the current volcanic activity. Improved locations using the new velocity model show two sub-clusters of activity: an EW-oriented group and a N148°E-oriented group. The distal cluster, and particularly the N148 group, probably highlights the pathway of magma propagation towards the surface eruptions. The lack of seismicity between the N148 group and the surface is consistent with continuous magma migration from a shallower (~17 km depth) reservoir to the seafloor lava flows.

Data and resources

The velocity model, station corrections and catalog presented in this study are available under the DOI 10.18715/IPGP.2021.kwdfof3p.

Data

RA network (Résif, 1995): YTMZ and MILA stations data available from Résif datacenter (http://seismology.resif.fr).

ED network: MCHI station data is available upon request at EduSismo.

1T network (Feuillet et al., 2022): land stations are from the Résif-Sismob pool of instruments and data is available upon request at Résif datacenter (Péquegnat et al., 2021).

The INSU-IPGP pool of OBS is managed and operated by IPGP and CNRS (https://parc-obs.insu.cnrs.fr/). MicrOBS and LotOBS are operated by IFREMER/Ressources Physiques et Ecosystèmes de fond de Mer/Département de Géosciences Marines/Service de Cartographie et Traitement de Données d'Instrumentation. Data is available upon request at IPGP datacenter (http://datacenter.ipgp.fr).

AM network (Raspberry Shake, 2016): R0CC5, R1EE2 and RAE55 stations data are acquired by Raspberry Shake SA company and made available from IRIS datacenter and Raspberry Shake SA datacenter.

Past felt earthquakes statistics on Mayotte from SisFrance database: http://www.sisfrance.net .

Ressources

ObsPy (Beyreuther et al., 2010) and GMT (Wessel et al., 2019) were used in analysing data and for figures. The VELEST (Kissling et al., 1995) and NonLinLoc (Lomax et al., 2000; Lomax et al., 2014) softwares were used respectively for the development of the velocity model and for earthquake locations, and are freely available. Calculation of the moment tensor mentioned in 5.2 was made by the Global Centroid Moment Tensor Project (GCMT) (Dziewonski et al., 1981; Ekström et al., 2012).

Author statement

A. Lavayssière developed the velocity model and station corrections and relocated all events, with the technical support of W. Crawford, J.-M. Saurel and C. Satriano. A. Lavayssière wrote the manuscript and created all figures with the contributions of all co-authors.

Declaration of Competing Interest

None.

Acknowledgments

We thank the REVOSIMA seismology group, BCSF/ReNaSS, and OVPF-IPGP for the picking of the data, discussion and support. We also thank Carole Berthod for her insights in the petrological discussion; and Anthony Lomax and one other anonymous reviewer for their constructive reviews in the improvement of this paper.

Since June 2019, all activities on Mayotte are funded by le Ministère de l'Enseignement Supérieur, de la Recherche et de l'Innovation (MESRI), le Ministère de la Transition Ecologique (MTE), le Ministère des Outremers (MOM), le Ministère de l'Intérieur (MI), and le Ministère des Armées with the support of the DIRMOM (Direction Interministérielle aux Risques Majeurs en Outremer). This project has also received funding from the Réseau de Surveillance Volcanologique et Sismologique de Mayotte (REVOSIMA) and from the European Union’s Horizon 2020 research and innovation program under grant agreement No 731070. All the OBS deployments and recoveries are performed as part of the MAYOBS set of cruises (doi:10.18142/291) and we thank the captains and crews of the R/V Marion Dufresne, R/V Pourquoi Pas?. R/V Champlain and LCT Ylang. Mayotte land-stations are maintained by CNRS/EOST/IPGS, BRGM and OVPF-IPGP and the OBS are recovered, maintained and data pre-processed by CNRS/INSU and IFREMER. We thank the IPGP for general funding to the Observatoires Volcanologiques et Sismologiques (OVS). The data contributes to the Service National d'Observation en Volcanologie (SNOV),This is IPGP contribution XXX and contributes to IdEx Université de Paris ANR-18-IDEX-0001.

Appendix A. Supplementary data

Supplementary data to this article can be found online at https://doi.org/10.1016/j.jvolgeores.2021.107440.

References

Acocella, V., 2007. Understanding caldera structure and development: an overview of analogue models compared to natural calderas. Earth Sci. Rev. 85 (3–4), 125–160.

Aloisi, M., Cocina, O., Neri, G., Orecchio, B., Privitera, E., 2002. Seismic tomography of the crust underneath the Etna volcano, Sicily. Phys. Earth Planet. Inter. 134 (3-4), 139–155.

Barruol, G., Deplus, C., Singh, S., 2012. MD 192/RHUM-RUM Cruise, RV Marion Dufresne. https://doi.org/10.17600/12200070.

Bassias, Y., Leclaire, L., 1990. The Davie Ridge in the Mozambique Channel: crystalline basement and intraplate magmatism. Neues Jahrb. Für Geol. Und Paläontologie-Monatshefte 67–90.

Berthod, C., Médard, E., Bachèlery, P., Gurioli, L., Di Muro, A., Peltier, A., Komorowski, J.-C., Benbakkar, M., Devidal, J.-L., Langlade, J., Besson, P., Boudon, G., Rose-Koga, E., Deplus, C., Le Friant, A., Bickert, M., Nowak, S., Thinon, I., Burckel, P., Hidalgo, S., Kaliwoda, M., Jorry, S., Fouquet, Y., Feuillet, N., 2021a. The 2018-ongoing Mayotte submarine eruption: Magma migration imaged by petrological monitoring. Earth Planet. Sci. Lett. 571.

Berthod, C., Médard, E., Di Muro, A., et al., 2021b. Mantle xenolith-bearing phonolites and basanites feed the active volcanic ridge of Mayotte (Comoros archipelago, SW Indian Ocean). Contrib. Mineral. Petrol. 176, 75. https://doi.org/10.1007/s00410-021-01833-1.

Bertil, D., Regnoult, J.M., 1998. Seismotectonics of Madagascar. Tectonophysics 294, 57–74.

Brocher, T.M., 2005. Empirical relations between elastic wavespeeds and density in the Earth's crust. Bull. Seismol. Soc. Am. 95, 2081–2092.

Cesca, S., Letort, J., Razafindrakoto, H.N.T., Heimann, S., Rivalta, E., Isken, M.P., Nikkhoo, M., Passarelli, L., Petersen, G.M., Cotton, F., 2020. Drainage of a deep magma reservoir near Mayotte inferred from seismicity and deformation. Nat. Geosci. 13, 87–93.

Chiarabba, C., Amato, A., Boschi, E., Barberi, F., 2000. Recent seismicity and tomographic modeling of the Mount Etna plumbing system. J. Geophys. Res. Solid Earth 105 (B5), 10923–10938.

Chiarabba, C., Moretti, M., 2006. An insight into the unrest phenomena at the Campi Flegrei caldera from Vp and Vp/Vs tomography. Terra Nova 18 (6), 373–379.

Christensen, N.I., 1996. Poisson's ratio and crustal seismology. J. Geophys. Res. Solid Earth 101, 3139–3156. https://doi.org/10.1029/95JB03446.

Clarke, D., Townend, J., Savage, M.K., Bannister, S., 2009. Seismicity in the Rotorua and Kawerau geothermal systems, Taupo Volcanic Zone, New Zealand, based on improved velocity models and cross-correlation measurements. J. Volcanol. Geotherm. Res. 180 (1), 50–66.

Claude-Ivanaj, C., Bourdon, B., Allègre, C.J., 1998. Ra–Th–Sr isotope systematics in Grande Comore Island: a case study of plume–lithosphere interaction. Earth Planet. Sci. Lett. 164, 99–117.

Coffin, M.F., Rabinowitz, P.D., Houtz, R.E., 1986. Crustal structure in the western Somali Basin. Geophys. J. Int. 86, 331–369.

Crosson, R.S., 1976. Crustal structure modeling of earthquake data: 1. Simultaneous least squares estimation of hypocenter and velocity parameters. J. Geophys. Res. 81, 3036–3046.

Davis, J.K., Lawver, L.A., Norton, I.O., Gahagan, L.M., 2016. New Somali Basin magnetic anomalies and a plate model for the early Indian Ocean. Gondwana Res. 34, 16–28.

Debeuf, D., 2004. Étude de L'évolution Volcano-Structurale et Magmatique de Mayotte (archipel des Comores, Océan Indien). Univ. la Reun, p. 277.

Dofal, A., Fontaine, F.R., Michon, L., Barruol, G., Tkalcic, H., 2018. Crustal structure variation across the southwestern Indian Ocean from receiver functions determined at Ocean-Bottom Seismometers. AGU Fall Meeting 2018. AGU.

Dofal, A., Fontaine, F.R., Michon, L., Barruol, G., Tkalcic, H., 2019. The hidden magma of the oceanic islands of the southwestern Indian Ocean from the study of receiver functions. Geophys. Res. Abstr. 21, 1 2019. 1p.

Dofal, A., Fontaine, F.R., Michon, L., Barruol, G., Tkalcic, H., 2021. Nature of the crust beneath the islands of the Mozambique Channel: constraints from receiver functions. J. Afr. Earth Sci. 184, 104379.

Dziewonski, A.M., Chou, T.-A., Woodhouse, J.H., 1981. Determination of earthquake source parameters from waveform data for studies of global and regional seismicity. J. Geophys. Res. 86, 2825–2852. https://doi.org/10.1029/JB086iB04p02825.

Ekström, G., Nettles, M., Dziewonski, A.M., 2012. The global CMT project 2004-2010: Centroid-moment tensors for 13,017 earthquakes. Phys. Earth Planet. Inter. 200-201, 1–9. https://doi.org/10.1016/j.pepi.2012.04.002.

Emerick, C.M., Duncan, R.A., 1982. Age progressive volcanism in the Comores Archipelago, western Indian Ocean and implications for Somali plate tectonics. Earth Planet. Sci. Lett. 60, 415–428.

Famin, V., Michon, L., Bourhane, A., 2020. The Comoros archipelago: a right-lateral transform boundary between the Somalia and Lwandle plates. Tectonophysics 789, 228539.

Feuillet, N., 2019. MAYOBS1 Cruise, RV Marion Dufresne. https://doi.org/10.17600/18001217.

Feuillet, N., Jorry, S., Rinnert, E., Thinon, I., Fouquet, Y., 2019. MAYOBS. https://doi.org/10.18142/291.

Feuillet, N., Jorry, S., Crawford, W., Deplus, C., Thinon, I., Jacques, E., Saurel, J.-M., Lemoine, A., Paquet, F., Satriano, C., Aiken, C., Foix, O., Kowalski, P., Laurent, A., Rinnert, E., Cathalot, C., Donval, J.-P., Guyader, V., Gaillot, A., Moreira, M., Peltier, A., Beauducel, F., Grandin, R., Ballu, V., Daniel, R., Pelleau, P., Besancon, S., Geli, L., Bernard, P., Bachelery, P., Fouquet, Y., Bertil, D., Lemarchand, A., Van der Woerd, J., 2021. Birth of a Large Volcanic Edifice Through Lithosphere-Scale Dyking Offshore Mayotte (Indian Ocean). https://doi.org/10.31223/X5B89P.

Feuillet, N., Van der Woerd, J., RESIF, 2022. Seismic Squence Monitoring on Land and at Sea in Mayotte: SISMAYOTTE (RESIF-SISMOB) [Data set]. RESIF - Réseau Sismologique et géodésique Français. https://doi.org/10.15778/resif.1t2018.

Filson, J., Simkin, T., Leu, L.K., 1973. Seismicity of a caldera collapse: Galapagos Islands 1968. J. Geophys. Res. 78 (35), 8591–8622.

Flower, M.F.J., Strong, D.F., 1969. The significance of sandstone inclusions in lavas of the Comores Archipelago. Earth Planet. Sci. Lett. 7, 47–50.

Geshi, N., Oikawa, T., 2008. Phreatomagmatic eruptions associated with the caldera collapse during the Miyakejima 2000 eruption, Japan. J. Volcanol. Geotherm. Res. 176 (4), 457–468.

Geyer, A., Martí, J., 2014. A short review of our current understanding of the development of ring faults during collapse caldera formation. Front. Earth Sci. 2, 22.

Gomberg, J.S., Shedlock, K.M., Roecker, S.W., 1990. The effect of S-wave arrival times on the accuracy of hypocenter estimation. Bull. Seismol. Soc. Am. 80, 1605–1628.

Gudmundsson, M.T., Jónsdóttir, K., Hooper, A., Holohan, E.P., Halldórsson, S.A., Ófeigsson, B.G., et al., 2016. Gradual caldera collapse at Bárdarbunga volcano, Iceland, regulated by lateral magma outflow. Science 353 (6296).

Guo, Q., Zhang, H., Han, F., Xiao, W., Shang, Z., 2018. A hybrid seismic inversion method for Vp/Vs ratio and its application to gas identification. Pure Appl. Geophys. 175 (8), 3003–3022.

Hajash, A., Armstrong, R.L., 1972. Paleomagnetic and radiometric evidence for the age of the Comores Islands, west Central Indian Ocean. Earth Planet. Sci. Lett. 16, 231–236.

Husen, S., Smith, R.B., Waite, G.P., 2004. Evidence for gas and magmatic sources beneath the Yellowstone volcanic field from seismic tomographic imaging. J. Volcanol. Geotherm. Res. 131, 397–410. https://doi.org/10.1016/S0377-0273(03)00416-5.

Jacques, E., Feuillet, N., Aiken, C., Lemoine, A., Crawford, W.C., Deplus, C., et al., 2019. The 2018-2019 Mayotte seismic crisis: evidence of an upper mantle rifting event? AGU Fall Meeting Abstracts. vol. 2019. AGU, pp. V43I–0221

Johnson, J.H., Poland, M.P., 2013. Seismic detection of increased degassing before Kilauea's 2008 summit explosion. Nat. Commun. 4, 1668.

Kennett, B.L.N., Engdahl, E.R., Buland, R., 1995. Constraints on seismic velocities in the Earth from traveltimes. Geophys. J. Int. 122, 108–124.

Kissling, E., 1988. Geotomography with local earthquake data. Rev. Geophys. https://doi.org/10.1029/RG026i004p00659.

Kissling, E., Kradolfer, U., Maurer, H., 1995. Program VELEST user's Guide-Short Introduction. Inst. Geophys. ETH Zurich.

Klimke, J., Franke, D., Gaedicke, C., Schreckenberger, B., Schnabel, M., Stollhofen, H., Rose, J., Chaheire, M., 2016. How to identify oceanic crust—evidence for a complex breakup in the Mozambique Channel, off East Africa. Tectonophysics 693, 436–452.

Lavayssière, A., 2019. Interactions between Tectonic and Magmatic Processes in the East African Rift.. (Doctoral dissertation)University of Southampton.

Leinweber, T., Klingelhoefer, F., Neben, S., Reichert, C., Aslanian, D., Matias, L., Heyde, I., Schreckenberger, B., Jokat, W., 2013. The crustal structure of the Central Mozambique continental margin—wide-angle seismic, gravity and magnetic study in the Mozambique Channel, Eastern Africa. Tectonophysics 599, 170–196.

Lemoine, A., Briole, P., Bertil, D., Roullé, A., Foumelis, M., Thinon, I., Raucoules, D., De Michele, M., Valty, P., Hoste Colomer, R., 2020. The 2018–2019 seismo-volcanic crisis east of Mayotte, Comoros islands: seismicity and ground deformation markers of an exceptional submarine eruption. Geophys. J. Int. 223, 22–44.

Lengliné, O., Duputel, Z., Ferrazzini, V., 2016. Uncovering the hidden signature of a magmatic recharge at Piton de la Fournaise volcano using small earthquakes. Geophys. Res. Lett. 43 (9), 4255–4262.

Lin, G., 2013. Seismic investigation of magmatic unrest beneath Mammoth Mountain, California, USA. Geology 41, 847–850. https://doi.org/10.1130/G34062.1.

Lin, G., Shearer, P.M., 2009. Evidence for water-filled cracks in earthquake source regions. Geophys. Res. Lett. 36. https://doi.org/10.1029/2009GL039098.

Lomax, A., Virieux, J., Volant, P., Berge, C., 2000. Probabilistic earthquake location in 3D and layered models: Introduction of a Metropolis-Gibbs method and comparison with linear locations. In: Thurber, C.H., Rabinowitz, N. (Eds.), Advances in Seismic Event Location. Kluwer, Amsterdam, pp. 101–134 https://doi.org/10.1007/978-94-015-9536-0_5.

Lomax, A., Michelini, A., Curtis, A., 2014. In: Meyers, R.A. (Ed.), Earthquake Location, Direct, Global-Search Methods, in Encyclopedia of Complexity and System Science, 2nd ed. Springer, New York, pp. 1–33 https://doi.org/10.1007/978-3-642-27737-5_150-2.

López, C., García-Cañada, L., Marti, J., Cerdena, I.D., 2017. Early signs of geodynamic activity before the 2011–2012 El Hierro eruption. J. Geodyn. 104, 1–14.

Malod, J.-A., Mougenot, D., Raillard, S., Maillard, A., 1991. Nouvelles contraintes sur la cinématique de Madagascar; les structures de la chaine Davie. Compt. Rend. Acad. Sci. 312, 1639–1646.

Matrullo, E., De Matteis, R., Satriano, C., Amoroso, O., Zollo, A., 2013. An improved 1-D seismic velocity model for seismological studies in the Campania–Lucania region (Southern Italy). Geophys. J. Int. 195 (1), 460–473.

Mavko, G., Mukerji, T., 1998. Bounds on low-frequency seismic velocities in partially saturated rocks. Geophysics 63, 918–924.

Michon, L., 2016. The volcanism of the Comoros archipelago integrated at a regional scale. Active Volcanoes of the Southwest Indian Ocean. Springer, pp. 333–344.

Nakajima, J., Matsuzawa, T., Hasegawa, A., Zhao, D., 2001. Three-dimensional structure of Vp, Vs, and Vp/Vs beneath northeastern Japan: implications for arc magmatism and fluids. J. Geophys. Res. Solid Earth 106, 21843–21857. https://doi.org/10.1029/2000JB000008.

Nougier, J., Cantagrel, J.M., Karche, J.P., 1986. The Comores archipelago in the western Indian Ocean: volcanology, geochronology and geodynamic setting. J. Afr. Earth Sci. 5, 135–145.

Pasyanos, M.E., Masters, T.G., Laske, G., Ma, Z., 2014. LITHO1. 0: an updated crust and lithospheric model of the Earth. J. Geophys. Res. Solid Earth 119, 2153–2173.

Patanè, D., Barberi, G., Cocina, O., De Gori, P., Chiarabba, C., 2006. Time-resolved seismic tomography detects magma intrusions at Mount Etna. Science 313 (5788), 821–823.
Pavlis, G.L., 1986. Appraising earthquake hypocenter location errors: a complete, practical approach for single-event locations. Bull. Seismol. Soc. Am. 76, 1699–1717.
Pelleter, A.-A., Caroff, M., Cordier, C., Bachèlery, P., Nehlig, P., Debeuf, D., Arnaud, N., 2014. Melilite-bearing lavas in Mayotte (France): an insight into the mantle source below the Comores. Lithos 208, 281–297.
Péquegnat, C., Schaeffer, J., Satriano, C., Pedersen, H., Touvier, J., Saurel, J.M., et al., 2021. RÉSIF-SI: a distributed information system for French seismological data. Seismol. Res. Lett. 92 (3), 1832–1853. https://doi.org/10.1785/0220200392.
Phethean, J.J.J., Kalnins, L.M., van Hunen, J., Biffi, P.G., Davies, R.J., McCaffrey, K.J.W., 2016. Madagascar's escape from Africa: a high-resolution plate reconstruction for the Western Somali Basin and implications for supercontinent dispersal. Geochem. Geophys. Geosyst. 17, 5036–5055. https://doi.org/10.1002/2016GC006624.
Poli, P., 2019. In between known earthquakes: Characteristics long period earthquakes from oceanic ridges and ultra-low frequency volcanic tremors. Geophysical Research Abstracts.
Priestley, K., McKenzie, D., 2006. The thermal structure of the lithosphere from shear wave velocities. Earth Planet. Sci. Lett. 244, 285–301. https://doi.org/10.1016/j.epsl.2006.01.008.
Rabinowitz, P.D., Coffin, M.F., Falvey, D., 1983. The separation of Madagascar and Africa. Science 80 (220), 67–69.
Raspberry Shake, S.A., 2016. Raspberry Shake [Data set]. International Federation of Digital Seismograph Networks. https://doi.org/10.7914/SN/AM.
REVOSIMA, 2021. Bulletin Mensuel du Réseau de surveillance volcanologique et sismologique de Mayotte. http://www.ipgp.fr/fr/revosima/actualites-reseau.
Rinnert, E., Feuillet, N., Fouquet, Y., Jorry, S., Thinon, I., Lebas, E., 2019. MAYOBS https://doi.org/10.18142/291.
Saria, E., Calais, E., Stamps, D.S., Delvaux, D., Hartnady, C.J.H., 2014. Present-day kinematics of the East African Rift. J. Geophys. Res. Solid Earth 119, 3584–3600. https://doi.org/10.1002/2013JB010901.
Satriano, C., Laurent, A., Bernard, P., Grandin, R., Saurel, J.-M., Lemarchand, A., Daniel, R., Jorry, S., Crawford, W.C., Feuillet, N., 2019. Source process of the very low frequency earthquakes during the Mayotte 2018-2019 seismo-volcanic crisis. AGU Fall Meeting Abstracts, pp. V43I–0222.
Saurel, J.M., Jacques, E., Aiken, C., Lemoine, A., Retailleau, L., Lavayssière, A., ... Feuillet, N., 2021a. Mayotte seismic crisis: building knowledge in near real-time by combining land and ocean-bottom seismometers, first results. Geophys. J. Int. 228 (2), 1281–1293.
Saurel, Jean-Marie, Jacques Eric, Aiken Chastity, Lemoine, Anne, Retailleau Lise, Lavayssière Aude, Foix Océane, Dofal Anthony, Laurent Angèle, Mercury Nicolas, Crawford Wayne, Lemarchand Arnaud, Romuald, Daniel, Pelleau Pascal, Bès de Berc Maxime, Dectot Grégoire, Bertil Didier, Roullé Agathe, Broucke Céleste, Thinon, Isabelle, b. https://doi.org/10.18715/IPGP.2021.kq136bzh.
Sauter, D., Ringenbach, J.C., Cannat, M., Maurin, T., Manatschal, G., McDermott, K.G., 2018. Intraplate deformation of oceanic crust in the West Somali Basin: insights from long-offset reflection seismic data. Tectonics 37, 588–603.
Segoufin, J., Patriat, P., 1981. Reconstructions de l'Ocean Indien Occidental pour les epoques des anomalies M21, M2 et 34; Paleoposition de Madagascar. Bull. Soc. Géol. Fr. 7, 603–607.
Sevilla, W.I., Jumawan, L.A., Clarito, C.J., Quintia, M.A., Dominguiano, A.A., Solidum Jr., R.U., 2020. Improved 1D velocity model and deep long-period earthquakes in Kanlaon Volcano, Philippines: implications for its magmatic system. J. Volcanol. Geotherm. Res. 393, 106793.
Stamps, D.S., Saria, E., Kreemer, C., 2018. A geodetic strain rate model for the East African Rift system. Sci. Rep. 8, 732. https://doi.org/10.1038/s41598-017-19097-w.
Talwani, M., 1962. Gravity measurements on HMS Acheron in South Atlantic and Indian Oceans. Geol. Soc. Am. Bull. 73, 1171–1182.
Thurber, C.H., 1983. Earthquake locations and three-dimensional crustal structure in the Coyote Lake area, Central California. J. Geophys. Res. Solid Earth 88, 8226–8236.
Unglert, K., Savage, M.K., Fournier, N., Ohkura, T., Abe, Y., 2011. Shear wave splitting, vP/vS, and GPS during a time of enhanced activity at Aso caldera, Kyushu. J. Geophys. Res. Solid Earth 116 (B11).
Wessel, P., Luis, J.F., Uieda, L., Scharroo, R., Wobbe, F., Smith, W.H.F., Tian, D., 2019. The generic mapping tools version 6. Geochem. Geophys. Geosyst. 20, 5556–5564. https://doi.org/10.1029/2019gc008515.
Woods, J., Winder, T., White, R.S., Brandsdóttir, B., 2019. Evolution of a lateral dike intrusion revealed by relatively-relocated dike-induced earthquakes: the 2014–15 Bárðarbunga–Holuhraun rifting event, Iceland. Earth Planet. Sci. Lett. 506, 53–63.
You, S.H., Gung, Y., Lin, C.H., Konstantinou, K.I., Chang, T.M., Chang, E.T.Y., Solidum, R., 2013. A preliminary seismic study of Taal Volcano, Luzon island Philippines. J. Asian Earth Sci. 65, 100–106.
You, S.H., Konstantinou, K.I., Gung, Y., Lin, C.H., 2017. Three-dimensional shallow velocity structure beneath Taal Volcano, Philippines. J. Seismol. 21 (6), 1427–1438.
Zhang, Q., Lin, G., 2014. Three-dimensional Vp and Vp/Vs models in the Coso geothermal area, California: seismic characterization of the magmatic system. J. Geophys. Res. Solid Earth 119, 4907–4922. https://doi.org/10.1002/2014JB010992.
Résif. 1995. Résif-RAP French Accelerometric Network, Résif - Réseau Sismologique etgéodésique Français. doi:10.15778/RESIF.RA